Numerical Heat Transfer, Part B, 60: 96–115, 2011

ISSN: 1040-7790 print/1521-0626 online
DOI: 10.1080/10407790.2011.594389

Taylor & Francis
Taylor & Francis Group

DEVELOPMENT OF A PARTICLE INTERACTION KERNEL FOR CONVECTION-DIFFUSION SCALAR TRANSPORT EQUATION

Chinlong Huang[1], Tony W. H. Sheu[1,2,3], Takuji Ishikawa[4], and Takami Yamaguchi[4]

[1]*Department of Engineering Science and Ocean Engineering, National Taiwan University, Taipei, Taiwan, Republic of China*

[2]*Taida Institute of Mathematical Science (TIMS), National Taiwan University, Taipei, Taiwan, Republic of China*

[3]*Center for Quantum Science and Engineering (CQSE), National Taiwan University, Taipei, Taiwan, Republic of China*

[4]*Department of Bioengineering and Robotics, Graduate School of Engineering, Tohoku University, Sendai, Japan*

In this study we derive a mathematically rigorous kernel function, which accounts for the interaction among particles, within the framework of the particle method, to predict a computationally more accurate solution for the convection-diffusion equation investigated at low as well as high Peclet numbers. Determination of the functional dependence of the kernel function on the distance vector between the particles is therefore a key to the success of the interaction model. The smoothed quantity for a scalar or for a vector at a particle location is mathematically identical to its collocated value provided that the kernel function is chosen as the delta function. Such a kernel is unfortunately not computable in a discrete context. Our guideline for developing the modified kernel function is therefore to make it closer to the delta function as much as possible in cases when diffusion dominates convection. To achieve this goal, we enforce five constraint conditions in a derivation of the kernel function for the pure diffusion equation. In addition, this kernel function has no effect on the particles outside of the disk, which has the user's specified radius r_e***. To mimic the delta function we demand that the developed kernel function at*** $r = r_e$ ***should smoothly approach zero. It is also desired to acquire the largest possible value for the kernel function near*** $r = 0$***. As flow convection prevailingly dominates its diffusion counterpart, particle interaction at the upstream side should be more favorably taken into account to avoid numerical oscillations due to convective instability. We present in this study a two-dimensional upwind kernel function to enhance numerical stability along the flow direction. The proposed upwind kernel function can render an exact solution for the investigated convection-diffusion equation in the limiting one-dimensional case. The proposed particle interaction model featuring the newly developed kernel function is validated through several problems that are amenable to analytical solutions or have available benchmark solutions. Analysis of the stability condition and spatial accuracy order of the proposed particle interaction model are also provided in details.***

Received 12 October 2010; accepted 11 May 2011.

The financial support of the National Science Council under Grants NSC96-2221-E-002-293-MY2 and NSC97-2628-M-002-022 and CQSE project 97R0066-69 are gratefully acknowledged. The second author also acknowledges the excellent resources provided by Tohoku University during his sabbatical leave.

Address correspondence to Tony W. H. Sheu, No. 1, Sec. 4, Roosevelt Road, Taipei, 10617, Taiwan, Republic of China. E-mail: twhsheu@ntu.edu.tw

NOMENCLATURE

B	stabilization term of the upwind-type kernel function	u	velocity component in the x direction
		v	velocity component in the y direction
d	number of dimensions	w	kernel function
f	dependent variable	W	upwind-type kernel function
h	distance between two particles	δ	delta function
i, j	particle indices	Δx	grid size in the x direction
n^0	particle number density	Δy	grid size in the y direction
Pe	Peclet number	μ	viscosity
r	particle location	τ	upwinding coefficient
r_e	radius of a small circle	ϕ	scalar function
s	local tangential direction		

1. INTRODUCTION

Techniques available for performing flow simulations can be divided into two classes, Eulerian and Lagrangian. For formulations within the Eulerian context, their partial differential equations are calculated on a fixed-mesh system. In Lagrangian methods, which can be subdivided into mesh-based and mesh-free methods, meshes or particles are not fixed to the domain but are instead advected with the fluid flow. The consequence that one no longer has a need to approximate the convection terms shown in the transport equations is now known as one of the apparent advantages of employing the Lagrangian approaches. Numerical errors of the cross-wind diffusion type can, in particular, be avoided accordingly. There exists, however, another mathematically rigorous arbitrary Lagrangian-Eulerian (ALE) method [1], which invokes both the Lagrangian and Eulerian steps in the course of moving a mesh.

Besides the well-known grid-based methods, such as the marker-and-cell (MAC) [2], volume-of-fluid (VOF) [3], and level-set [4] methods applied to predict free-surface problems with great success, there exist another major class of successful mesh-free methods, known as the particle methods. Particle methods feature the prescribed particles moving in Lagrangian coordinates such that the convection terms can be calculated directly from the motion of the particles without incurring any numerical diffusion. Particle methods can be also separated into the Eulerian particle methods, such as the particle-in-cell (PIC) method [5], and the Lagrangian particle methods, which include smoothed particle hydrodynamics (SPH) method, and the moving-particle semi-implicit (MPS) method, two major types of meshless methods. The SPH method, introduced first by Lucy [6] and by Gingold and Monaghan [7] at about the same time in 1977, was developed mainly for the simulation of compressible fluid flows based on the interpolation theory through the introduced kernel function (or smoothing kernel). The SPH method was later extended to simulate also the incompressible free-surface flow [8].

The MPS method was developed more recently to simulate incompressible Navier-Stokes fluid flows [9]. In this method the motion of each particle is calculated through the interaction with its neighboring particles by means of the kernel (or weight) function. This means that all the spatial derivatives can be calculated by

the deterministic particle interaction in the flow, without the need to generate grids. This explains why the MPS method has gradually become quiet effective for use in simulating many problems involving either complicated geometry or complex physics. For problems with inflow or outflow boundaries, however, this method was found to be difficult to trace a particle easily. In addition, the MPS method requires additional computational time to find all the neighboring points. In the literature about the MPS method, one can find the particle-gridless hybrid method by Yoon et al. [10] and the hybrid particle-mesh method by Liu et al. [11]. Ataie-Ashtiani and Farhadi [12] investigated several kernel functions for improving the stability of the MPS method. Hibi and Yabushita [13] and Sueyoshi [14] introduced an additional procedure to obtain a smooth pressure. Khayyer and Gotoh [15, 16] improved the MPS method with the aim of ensuring momentum conservation. Kondo and Koshizuka [17] recently proposed a new MPS formulation for the source term in the pressure Poisson equation to improve stability.

While the MPS method has been used for more than a decade to simulate low-speed complex flow physics with great success, its computational insight has been less explored. Questions regarding the reduced accuracy as the grids are increasingly refined and the slow convergence when simulating a slightly higher Peclet number flow have been often raised. For this reason, we will simplify the analysis in this study by considering first the stationary particle method so that more theoretical insights may be gained through the analysis of the proposed particle method. Application of the present kernel function to simulate moving-particle problems using the MPS and SPH methods needs more studies.

The rest of this article is organized as follows. In Section 2 we present the passive scalar equation, which involves the convection and diffusion fluxes, in a constant-coefficient flow. This is followed by presenting the particle interaction model for approximating the gradient and Laplacian differential operators. Emphasis in Section 4 is on the kernel function used in the particle method. In Section 5, we validate the proposed particle model by solving the convection-diffusion equation, which is amenable to analytic solutions. Several benchmark problems involving the smoothly varying, interior layer, and boundary-layer solutions will be also investigated in this study for the sake of validation. In Section 6, some conclusions are drawn based on the predicted results.

2. WORKING EQUATION

We consider in this study the following convection-diffusion scalar equation in a simply connected domain Ω:

$$u\frac{\partial \phi}{\partial x} + v\frac{\partial \phi}{\partial y} = \mu\left(\frac{\partial^2 \phi}{\partial x^2} + \frac{\partial^2 \phi}{\partial y^2}\right) \tag{1}$$

This model equation is considered since it is the key to performing numerical simulation of the incompressible momentum equations. Both velocity components u and v, and the viscosity μ, are assumed to be constant. This facilitates the current kernel function development in Section 4.

3. DETERMINISTIC PARTICLE INTERACTION MODELS FOR DIFFERENTIAL OPERATORS

Due to the difficulties of applying the grid-based methods to predict large-scale problems and simulate complex physics involving, for example, multiphases and fluid mixing, particle-based methods gradually became popular in the simulation of incompressible Navier-Stokes equations subject either to a free surface or to an interface in the flow domain. In particle methods, the differential operators for mass and momentum conservations shown in Section 2 need to be replaced by their corresponding particle interaction operators. In other words, partial differential equations cast in continuous context will be transformed to their corresponding particle interaction equations so that the transport equations under investigation can be approximated by moving or stationary particles and their interactions. One key issue in determining the degree of success is the selection of the kernel (or weighting) function for the particles that are distanced by the user's prescribed finite lengths. The indispensible kernel function acts as the smoothing function for the invoked physical quantities, such as the velocity vectors and pressure in the incompressible fluid flow around the particles.

Consider a particle i, for which some physical quantities f_i exist, at the coordinate $\underline{r}_i$. One can represent f_i at each location $\underline{r}$ approximately as follows by virtue of the kernel function $w(\underline{r})$ [6]:

$$\langle f(\underline{r})\rangle \cdot \sum_i w(|\underline{r}_i - \underline{r}|) = \sum_i f_i w(|\underline{r}_i - \underline{r}|) \tag{2}$$

In mathematics, the smoothed quantity $\langle f\rangle_i$ for f at the particle location $\underline{r}_i$ turns out to be exactly identical to the local value of f_i if the kernel function shown above is chosen to be the delta function. This implies that the chosen kernel function $w(\underline{r})$, which should be constrained by $\int_V w(r)\,dv = 1$, shown in (2) determines the prediction accuracy of the particle methods employed. One can find different variants of the kernel function in [12].

Considering a scalar ϕ at a location $\underline{r}_j$, one can express its value in Taylor series expansion with respect to the value of ϕ at the location $\underline{r}_i$ as follows:

$$\phi_j = \phi_i + \nabla\phi|_{ij} \cdot (\underline{r}_j - \underline{r}_i) + \text{HOT} \tag{3}$$

By dropping the higher-order terms shown above, we obtain the first-order approximated equation given by $\phi_j - \phi_i = \nabla\phi|_{ij} \cdot (\underline{r}_j - \underline{r}_i)$. By multiplying $(\underline{r}_j - \underline{r}_i)^{-1}$ on both sides of the above equation, we get

$$\nabla\phi|_{ij} = \frac{(\phi_j - \phi_i)(\underline{r}_j - \underline{r}_i)}{|\underline{r}_j - \underline{r}_i||\underline{r}_j - \underline{r}_i|} \tag{4}$$

Letting $\nabla\phi|_{ij} = f$ and substitute this equation into Eq. (2), we get the following smoothed representation of $\nabla\phi$, which is denoted as $\langle\nabla\phi\rangle$ at the node ij, for the case

with d dimension [9]:

$$\langle \nabla \phi \rangle|_{ij} = \frac{d}{n^0} \sum_{j \neq i} \frac{\phi_j - \phi_i}{|\underline{r}_j - \underline{r}_i|^2} (\underline{r}_j - \underline{r}_i)\, w(\underline{r}_j - \underline{r}_i) \tag{5}$$

In the above, n^0 denotes the particle number density and is defined as $\sum_{j \neq i} w(|\underline{r}_j - \underline{r}_i|)$. Note that $n_i = n^0$, which holds true for incompressible flow, is considered.

One can similarly derive the Laplacian of a scalar ϕ, which has been given in [18], as follows:

$$\langle \nabla^2 \phi \rangle|_{ij} = \frac{2d}{n^0} \sum_{j \neq i} \frac{\phi_j - \phi_i}{|\underline{r}_j - \underline{r}_i|^2}\, w(|\underline{r}_j - \underline{r}_i|) \tag{6}$$

One can also get the following smoothed representation of the Laplacian operator for $\langle \nabla^2 \phi \rangle_i$ [9]:

$$\langle \nabla^2 \phi \rangle|_i = \frac{2d}{\lambda n^0} \sum_{j \neq i} (\phi_j - \phi_i)\, w(|\underline{r}_j - \underline{r}_i|) \tag{7}$$

where

$$\lambda = \frac{\int_{V'} |\underline{r}_j - \underline{r}_i|^2\, w(|\underline{r}_j - \underline{r}_i|)\, dV}{\int_{V'} w(|\underline{r}_j - \underline{r}_i|)\, dV} \tag{8}$$

Note that V' is the volume excluding of a small interval that contains the point at i. It is worth pointing out here that the advantage of employing particle methods is that all spatial derivatives can be calculated from the chosen kernel function without mesh generation. Considerable effort in generating a good-quality mesh for an accurate numerical simulation in a stationary or moving domain is therefore avoided.

Unlike the SPH particle method, calculation of $\nabla \phi$ and $\nabla^2 \phi$ in Eqs. (5)–(7) involves only the kernel function $w(\underline{r})$. Since no differentiation of the kernel function is needed, numerical oscillations, which may be generated in the traditional fixed-grid Eulerian approach for solving problems with high solution gradients, can be completely avoided. As a result, one has more flexibility to choose a kernel function that can have a slope as steep as the delta function.

4. DEVELOPMENT OF KERNEL FUNCTIONS

As the particle interaction models show for $\langle \nabla \phi \rangle_{ij}$ and $\langle \nabla^2 \phi \rangle_i$ in Eqs. (5)–(7), the quality of these approximations depends entirely on the chosen kernel function $w(\underline{r})$ and the number distribution of the prescribed particles, which will affect $\underline{r}_i$. In addition, the chosen particle locations and kernel function determine the subsequent particle location. The prediction quality therefore depends largely on the chosen kernel function, which will be derived in detail.

In the light of Eq. (2), delta function $\delta(\underline{r})$, which is constrained by $\int_{-\infty}^{\infty} \delta(\underline{r})\, dr = 1$, is a good candidate for the chosen kernel function. This kernel

function is, however, not implementable in computation practice. We therefore have to resort to a smoothed delta function when carrying out simulations based on the particle method. The smoothed delta function is sometimes called a nascent delta function $\delta_\varepsilon(\underline{r})$, which is defined as $\lim_{\varepsilon \longrightarrow 0} \delta_\varepsilon(\underline{r}) = \delta(\underline{r})$. In the literature, there are several nascent delta functions for choice, such as the Gaussian function, Lorentz line function, impulse function and sinc function, etc. There exists also another class of kernel functions. They were developed indepently of the nascent delta functions. Typical examples include the exponential, cubic spline, and quadratic spline functions proposed by Belytschko et al. [19], and the kernel functions proposed by the group of Koshizuka in 1996 [20] and 1998 [21].

4.1. Center-Type Kernel Function for the Pure Diffusion Equation

In this study a new kernel function will be developed so that we can rigorously apply it to simulate the incompressible Navier-Stokes equations in the future using moving-particle methods. Our design guidelines to develop the proposed kernel function are given below. The kernel function $w(\underline{r})$ under current development falls into the category of nascent delta functions. This implies that $\lim_{r_e \longrightarrow 0} w(\underline{r}, r_e) = \delta(\underline{r})$, where r_e is the radius of a small circle. The weight between two arbitrary particles that are a distance r apart will be diminished as $r \geq r_e$. For the sake of accuracy, the kernel function will be developed to retain the characteristics of the delta function in the sense that

$$\int_{-\infty}^{\infty} w(\underline{r}, r_e)\, d\underline{r} = 1 \tag{9}$$

Development of the current kernel function starts with representing it in terms of the ratio r/r_e as

$$w(r) = \begin{cases} \frac{a}{r_e} + \frac{b}{r_e}\left(\frac{r}{r_e}\right) + \frac{c}{r_e}\left(\frac{r}{r_e}\right)^2 + \frac{d}{r_e}\left(\frac{r}{r_e}\right)^3 + \frac{e}{r_e}\left(\frac{r}{r_e}\right)^4 & 0 \leq r \leq r_e \\ 0 & r_e < r \end{cases} \tag{10}$$

Derivation of $w(\underline{r})$ is followed by imposing the four constraint conditions given by

$$w(r = r_e) = \left.\frac{\partial w}{\partial r}\right|_{r=r_e} = \left.\frac{\partial w}{\partial r}\right|_{r=0} = 0 \quad \text{and} \quad \int_0^{r/r_e=1} w(r)\, dr = \frac{1}{2}$$

These imposed conditions enable us to derive the algebraic equations given below:

$$a + b + c + d + e = 0 \tag{11}$$

$$b + 2c + 3d + 4e = 0 \tag{12}$$

$$a + \frac{b}{2} + \frac{c}{3} + \frac{d}{4} + \frac{e}{5} = \frac{1}{2} \tag{13}$$

$$b = 0 \tag{14}$$

From the above four equations, one can then easily express a, b, c, d in terms of e as

$$a = 1 - \frac{1}{15}e \quad b = 0 \quad c = -3 + \frac{6}{5}e \quad d = 2 - \frac{32}{15}e$$

By substituting the resulting kernel function into Eq. (6) for $\nabla^2\phi$, one can derive the corresponding discrete equation for the Laplace equation $\partial^2\phi/\partial x^2 + \partial^2\phi/\partial y^2 = 0$ in a grid with uniform mesh size h based on the particle method:

$$\frac{1}{[w(h) + 2w(\sqrt{2}h)]h^2}\{(\phi_{i+1,j} + \phi_{i-1,j} + \phi_{i,j+1} + \phi_{i,j-1} - 4\phi_i)\, w(h) + (\phi_{i+1,j+1} + \phi_{i-1,j+1} + \phi_{i+1,j-1} + \phi_{i-1,j-1} - 4\phi_i)\, w(\sqrt{2}h)\} = 0 \tag{15}$$

By performing the modified equation analysis on Eq. (15), the following modified equation can be derived:

$$\frac{\partial^2\phi}{\partial x^2} + \frac{\partial^2\phi}{\partial y^2} = -\left[\frac{w(\sqrt{2}h)}{w(h) + 2w(\sqrt{2}h)}\frac{\partial^4\phi}{\partial x^2\partial y^2} + \frac{1}{12}\frac{\partial^4\phi}{\partial x^4} + \frac{1}{12}\frac{\partial^4\phi}{\partial y^4}\right]h^2 - \left[\frac{w(\sqrt{2}h)}{12(w(h) + 2w(\sqrt{2}h))}\left(\frac{\partial^6\phi}{\partial x^4\partial y^2} + \frac{\partial^6\phi}{\partial x^2\partial y^4}\right) + \frac{1}{360}\frac{\partial^6\phi}{\partial x^6} + \frac{1}{360}\frac{\partial^6\phi}{\partial y^6}\right]h^4 + \ldots \tag{16}$$

Letting $w(\sqrt{2}h) = 1/4w(h)$, the first term on the right-hand side of (16) turns out to be

$$\frac{-1}{12}\left(\frac{\partial^4\phi}{\partial x^4} + 2\frac{\partial^4\phi}{\partial x^2\partial y^2} + \frac{\partial^4\phi}{\partial y^4}\right)h^2$$

which is equal to zero because $\left(\partial^2\phi/\partial x^2\right) + \left(\partial^2\phi/\partial y^2\right) = 0$.

Provided that $r_e = 2h$, we can easily see from the following nine-point stencil equation that the resulting approximated equation for (1) at $\mu = \infty$ has fourth-order accuracy:

$$\frac{\phi_{i+1,j+1} + \phi_{i-1,j+1} + \phi_{i-1,j+1} + \phi_{i+1,j-1} + 4\phi_{i+1,j} + 4\phi_{i-1,j} + 4\phi_{i,j+1} + 4\phi_{i,j-1} - 20\phi_{i,j}}{6h^2} + O(h^4) = 0 \tag{17}$$

Note that Eq. (17) is derived under the condition of

$$3a + \left(2\sqrt{2} - \frac{1}{2}\right)b + \left(2 - \frac{1}{4}\right)c + \left(\sqrt{2} - \frac{1}{8}\right)d + \left(1 - \frac{1}{16}\right)e = 0 \tag{18}$$

The resulting five free parameters can then be uniquely calculated from Eqs. (11)–(14) and (18) as

$$a = \frac{480\sqrt{2} - 705}{512\sqrt{2} - 745} \quad b = 0 \quad c = \frac{-960\sqrt{2} + 1,515}{512\sqrt{2} - 745}$$
$$d = \frac{-210}{512\sqrt{2} - 745} \quad e = \frac{480\sqrt{2} - 600}{512\sqrt{2} - 745}$$

In summary, the developed kernel function is as given below for the calculation of the pure diffusion equation:

$$w(r) = \begin{cases} \frac{480\sqrt{2}-705}{512\sqrt{2}-745}\frac{1}{r_e} + \frac{-960\sqrt{2}+1515}{512\sqrt{2}-745}\frac{1}{r_e}\left(\frac{r}{r_e}\right)^2 + \frac{-210}{512\sqrt{2}-745}\frac{1}{r_e}\left(\frac{r}{r_e}\right)^3 + \frac{480\sqrt{2}-600}{512\sqrt{2}-745}\frac{1}{r_e}\left(\frac{r}{r_e}\right)^4 & 0 \le r \le r_e \\ 0 & r_e < r \end{cases} \tag{19}$$

provided that

$$w(\sqrt{2}h) = \frac{1}{4}w(h) \tag{20}$$

Unlike the kernel function $w(r) = (r_e/r) - 1$ given in [20], which diverges as r approaches zero, our developed kernel function can be well defined and has its maximum value at $r = 0$. It is also worth restating that the currently developed kernel function used for prediction of the pure diffusion equation satisfies the following constraint condition, which is also embedded in the delta function:

$$\int_{r/r_e=-1}^{r/r_e=1} w(r)\, dr = 1 \tag{21}$$

4.2. Upwind-Type Kernel Function for the Convection-Diffusion Equation

As Figure 1 shows, Eq. (19) developed within the framework of delta function belongs to the center-type kernel functions, since fluid particles distanced from the reference node with the same length will impose the same influence (or weight) on that reference node. Such an interaction model will be physically reasonable only in the diffusion-dominant case [or if $\mathrm{Pe}(\equiv |\underline{u}|h/\mu) < 2$], where μ denotes the fluid viscosity. In science and engineering problems, the value of the Peclet number Pe is normally much larger than 2. Application of the kernel function developed in Section 4.1 and other published kernel functions in [19–21] to simulate a practical flow problem may result in a nonphysical pattern of oscillations due to the convective instability. To resolve this numerical problem, we must take the physics of fluid flow into consideration in the development of the necessary kernel function in particle methods.

Our idea of suppressing oscillatory solutions generated by the convective numerical instability is to implicitly add an appropriate amount of damping along

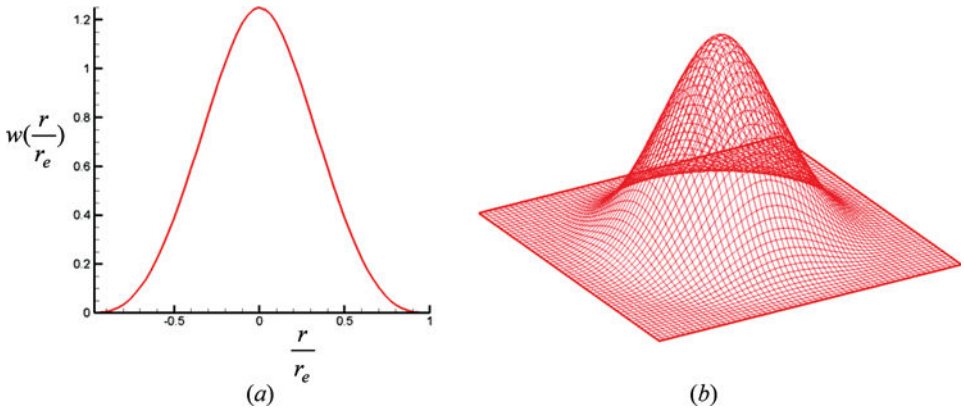

Figure 1. Plots of center-type kernel function developed for the Laplace equation: (*a*) plotted in r/r_e coordinates; (*b*) plotted in xy plane (color figure available online).

the flow direction when developing the kernel function. Considering a flow with the local velocity vector (u, v), the damping term along its local tangential direction $s\left[\equiv \tan^{-1}(v/u)\right]$ is ϕ_{ss}. By virtue of the relation

$$\phi_{ss} = \frac{u^2}{u^2+v^2}\phi_{xx} + \frac{v^2}{u^2+v^2}\phi_{yy} + \frac{2uv}{u^2+v^2}\phi_{xy} \tag{22}$$

we know that the kernel function derived to model a high-Peclet-number flow must have the ability to implicitly generate the damping terms in the x and $y$directions or explicitly add the damping terms to Eq. (1). Addition of such damping terms helps to stabilize the discrete equation for (1).

In this study we will modify the kernel function (19) developed for the simulation of transport equations at low Peclet numbers by adding a stabilization term to the kernel function (19). To get the terms like ϕ_{xx} and ϕ_{yy} for the sake of stabilization, we will change the center-type kernel function by adding a new term that can bring the required numerical stabilization mechanism into the particle method. The following upwind-type kernel function is therefore proposed:

$$W_i(r) = w_i(r) + B_i(r) \tag{23}$$

In the above, $w(r)$is the kernel function and the stabilization term is chosen to have the form

$$B_i(r) = \tau\, u^k \left|_i \frac{\partial w|_i}{\partial x^k}\right. \tag{24}$$

One can easily show that the inclusion of the velocity vector and gradient of the kernel function shown in (24) can render a second-order damping term ϕ_{ss} along the flow direction s. Note that the so-called crosswind diffusion term ϕ_{xy} will also be introduced in this formulation. Owing to the presence of ϕ_{xy}, we are motivated to

develop a scheme as accurately as possible so that the undesirable false diffusion error can be reduced or minimized. The consequence is that τ, which is known to determine the degree of upwinding, needs to be properly derived.

For the sake of accuracy, the upwinding coefficient τ shown in Eq. (24) will be developed in the limiting one-dimensional sense, since the resulting equation is amenable to exact solution. Take the following one-dimensional equation as an example in the following derivation of τ:

$$u\frac{\partial\phi}{\partial x} = \mu\frac{\partial^2\phi}{\partial x^2} \tag{25}$$

One can substitute Eqs. (5), (6), (19), and (23)–(24) into Eq. (25) to derive the discrete equation at a node i:

$$u\frac{\phi_{i+1} - \phi_{i-1}}{2\,\Delta x} - \mu\left[1 + \frac{\tau\,\Delta x\,u^2\,w'(\Delta x)}{2\mu\,w(\Delta x)}\right]\left(\frac{\phi_{i+1} - 2\phi_i + \phi_{i-1}}{\Delta x^2}\right) = 0 \tag{26}$$

By comparing the following exact equation for (25),

$$u\frac{\phi_{i+1} - \phi_{i-1}}{2\,\Delta x} - \frac{u\,\Delta x}{2}\coth\left(\frac{u\,\Delta x}{2\mu}\right)\left(\frac{\phi_{i+1} - 2\phi_i + \phi_{i-1}}{\Delta x^2}\right) = 0 \tag{27}$$

one can derive the upwinding coefficient τ in terms of the parameter $\gamma(\equiv u\,\Delta x/2\mu)$ given as follows:

$$\tau = \frac{w_i(\Delta x)}{uw_i'(\Delta x)}\frac{\gamma\coth(\gamma) - 1}{\gamma} \tag{28}$$

By expanding $\phi_{i+1,\,j+1}$, $\phi_{i+1,\,j-1}$, $\phi_{i-1,\,j+1}$, $\phi_{i-1,\,j-1}$, $\phi_{i-1,\,j}$, $\phi_{i+1,\,j}$, $\phi_{i,\,j+1}$, and $\phi_{i,\,j-1}$ in Taylor series with respect to $\phi_{i,\,j}$ and then substituting them into the discrete equation for (1), we can easily derive the following modified equation:

$$u\frac{\partial\phi}{\partial x} + v\frac{\partial\phi}{\partial y} - \mu\left(\frac{\partial^2\phi}{\partial x^2} + \frac{\partial^2\phi}{\partial y^2}\right) = a\frac{\partial^2\phi}{\partial x^2} + b\frac{\partial^2\phi}{\partial x\,\partial y} + c\frac{\partial^2\phi}{\partial y^2} + \ldots \tag{29}$$

Let

$$m = \frac{4(-512\sqrt{2} + 745)}{1,125(32\sqrt{2} - 47)}\frac{\gamma\coth(\gamma) - 1}{\gamma}\,\Delta x^2$$

Then the coefficients of the leading error terms shown above are expressed as

$$a = \frac{9u^2 + v^2}{\sqrt{u^2 + v^2}}m \tag{30}$$

$$b = \frac{4uv}{\sqrt{u^2 + v^2}}m \tag{31}$$

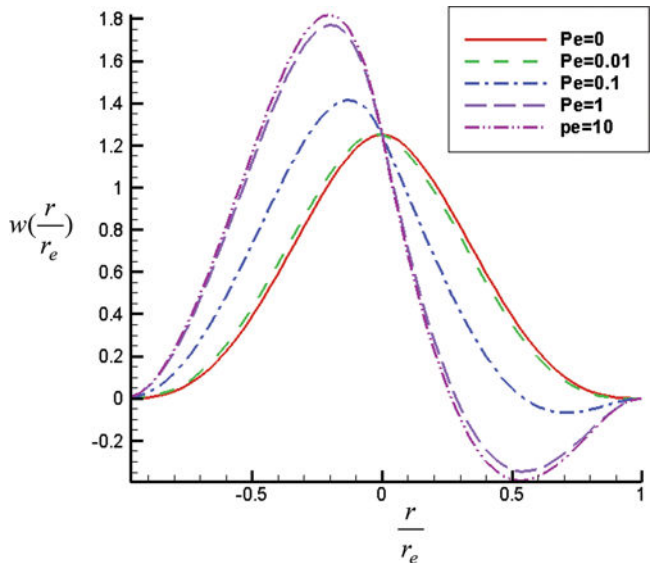

Figure 2. Upwind-type kernel function plotted at $u = 1$, $v = 1$, and different Peclet numbers 0, 0.01, 0.1, 1, and 10 (color figure available online).

$$c = \frac{u^2 + 9v^2}{\sqrt{u^2 + v^2}} m \tag{32}$$

Through the above-modified equation analysis, we know from the derived expression of m and (29)–(32) that the stability of the proposed scheme has been enhanced mainly along the streamline direction. The gain in stability enhancement is at the sacrifice of decreasing the accuracy order by two, in comparison with the fourth-order-accurate center-type interaction model derived in Section 4.1.

To make a clear comparison of the developed center and upwind kernel functions, the upwind-type kernel function recommended for use in the high-Peclet-number flow simulation is also plotted. In Figure 2, $w(\Delta x = r)$ is plotted for the case investigated, for example, at $u = v = 1$, and at different values of μ that could render respectively Pe = 0, 0.01, 0.1, 1, and 10.

5. NUMERICAL RESULTS

Several problems regarding the transport of ϕ, governed by Eq. (1), will be solved for the sake of analytically verifying the proposed particle method. The first problem deals with the Laplace equation in a unit square, which has been uniformly discretized in the domain with different mesh sizes $\Delta x = \Delta y = 0.25, 0.1666, 0.125, 0.1$. Calculation of this elliptic equation, subject to the boundary condition given by the analytic solution $\phi = \tan^{-1}[(x-2)/(y-2)]$, will be carried out. We tabulate the predicted L_2-error norms in Table 1, from which we can see that the predicted rate of convergence is surprisingly larger than its theoretical spatial rate, which is fourth, due possibly to machine error.

Table 1. Predicted L_2-error norms and corresponding rates of convergence by solving the Laplace equation, based on four different kernel functions, in different meshes

Mesh	Bell-shaped function [10]	Rational function [21]	Spiky function [22]	Center-type function (present)	Rate of convergence (present)
5×5	1.012×10^{-4}	1.056×10^{-3}	8.338×10^{-6}	1.811×10^{-8}	
7×7	7.863×10^{-5}	7.880×10^{-4}	5.568×10^{-6}	1.571×10^{-9}	7.26584
9×9	6.303×10^{-5}	6.221×10^{-4}	4.174×10^{-6}	2.681×10^{-10}	7.03544
11×11	5.238×10^{-5}	5.129×10^{-4}	3.345×10^{-6}	6.674×10^{-11}	6.92954

The next problem under current investigation involves solving the following smoothly distributed analytic solution, defined in $0 \leq x, y \leq 1$, for Eq. (1).

$$\phi = \frac{(1 - e^{(x-1)u/\mu})(1 - e^{(y-1)v/\mu})}{(1 - e^{-u/\mu})(1 - e^{-v/\mu})} \tag{33}$$

Calculation will be carried out first at the fixed value of Peclet number Pe ($\equiv u\,\Delta x/\mu$) $= 10^{-5}$, where Δx denotes the grid size, to justify the developed center-type kernel function. The solutions predicted at $\mu = 10^4$ using the center-type kernel function given in (19) are seen to agree excellently with the exact solution plotted in Figure 3. This confirms that the proposed kernel function is applicable to solve a problem with a Peclet number smaller than 2. Calculation is followed by solving Eq. (1) in different meshes. As Table 2 shows, the predicted solutions agree quite well with the theoretical solution and have higher accuracy than those shown in [9, 21, 22] for the case investigated at $\mu = 10^4$ using the center-type kernel function.

We then solve the same problem using the upwind-type kernel function at a smaller value of μ, say, at $\mu = 10^{-2}$, to make the equation a convection-dominated

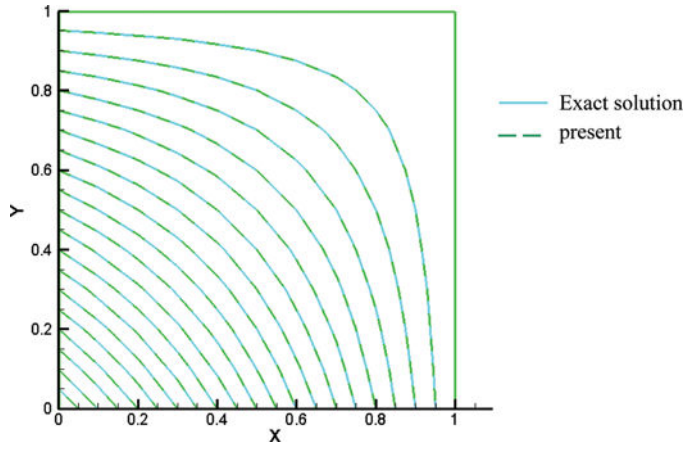

Figure 3. Comparison of exact solution with predicted solution at Pe $= 1 \times 10^{-3}$ based on the proposed center-type kernel function (color figure available online).

Table 2. Predicted L_2-error norms and corresponding rates of convergence by solving the convection-diffusion equation at $\mu = 10^4$, based on four different kernel functions, in different meshes

Mesh	Bell-shaped function [10]	Rational function [21]	Spiky function [22]	Center-type function (present)
10×10	8.534×10^{-5}	8.225×10^{-4}	4.847×10^{-6}	3.890×10^{-14}
20×20	4.531×10^{-5}	4.352×10^{-4}	2.587×10^{-6}	9.455×10^{-15}
30×30	3.083×10^{-5}	2.959×10^{-4}	1.763×10^{-6}	5.511×10^{-15}
40×40	2.336×10^{-5}	2.241×10^{-4}	1.337×10^{-6}	5.350×10^{-15}
50×50	1.881×10^{-5}	1.804×10^{-4}	1.076×10^{-6}	2.406×10^{-15}

Table 3. Predicted L_2-error norms and corresponding rates of convergence using the center-type and upwind-type kernel functions for Eq. (1) investigated at $\mu = 10^{-2}$

Mesh	L_2-error norm, center-type	L_2-error norm, upwind-type	Rate of convergence, upwind-type
60×60	1.859×10^{-2}	1.612×10^{-2}	
70×70	1.337×10^{-2}	1.188×10^{-2}	1.97991
80×80	1.006×10^{-2}	9.088×10^{-3}	2.00628
90×90	7.828×10^{-3}	7.163×10^{-3}	2.02089
100×100	6.263×10^{-3}	5.788×10^{-3}	2.02298

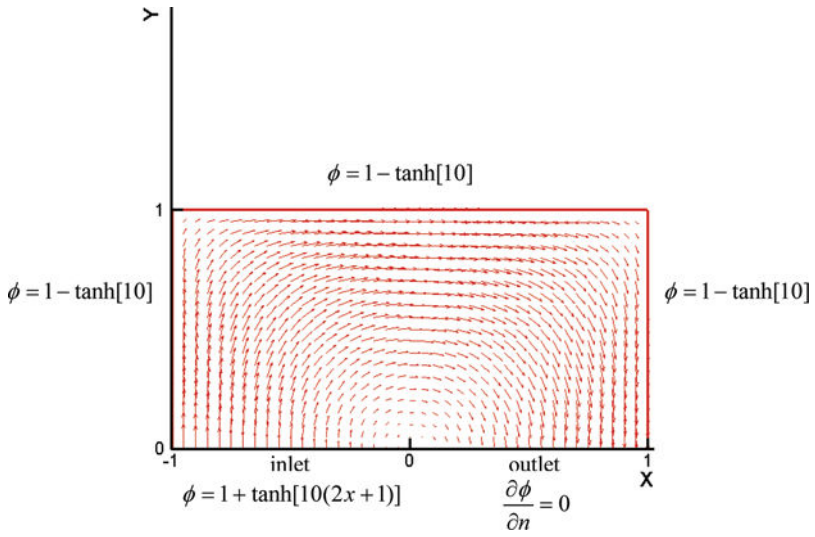

Figure 4. Schematic of boundary conditions and initially prescribed velocity vectors for the Smith and Hutton problem (color figure available online).

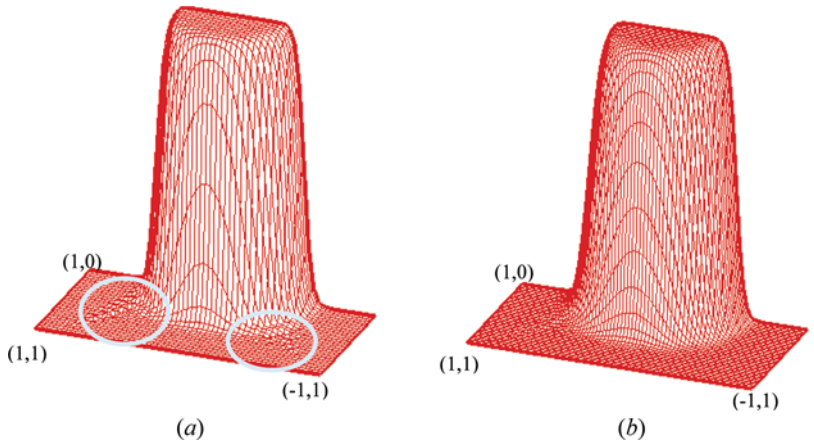

Figure 5. Illustration of the three-dimensional plot of the predicted ϕ using two different kernel functions for the Smith and Hutton problem investigated at $\mu = 10^{-4}$: (*a*) oscillatory solution (see the circled area) using the center-type kernel function; (*b*) smooth solution using the upwind-type kernel function (color figure available online).

one. The rates of convergence, tabulated in Table 3, are computed from the L_2-error norms of the solutions calculated from the upwind-type kernel function. Under our expectation, the predicted rates of convergence are approximately equal to two, due to the addition of the numerical damping terms shown in (29)–(32).

Verification of the proposed particle models is followed by solving two analytic problems, one involving an interior layer and the other involving interior as well as boundary layers, in cases of high Peclet numbers.

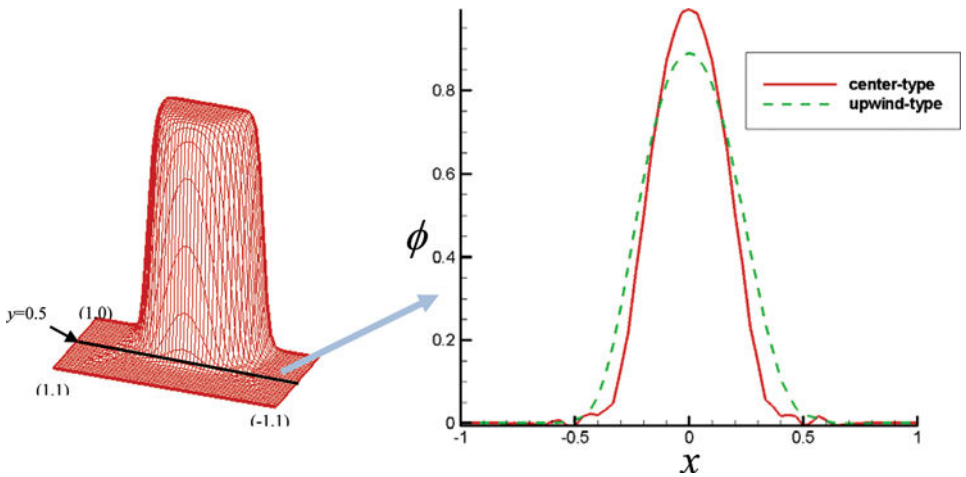

Figure 6. Comparison of results along the line $y = 0.5$ obtained from the center-type and upwind-type kernel functions for the Smith and Hutton problem investigated at $\mu = 10^{-4}$ (color figure available online).

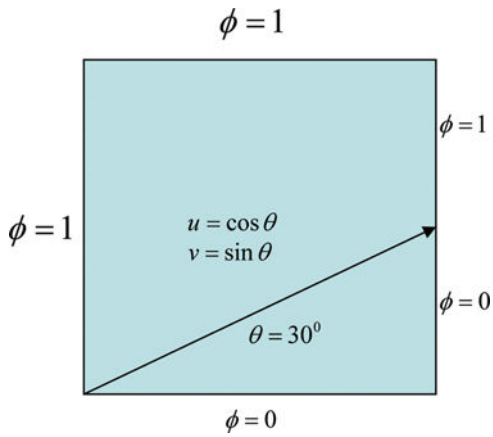

Figure 7. Schematic of skew convection-diffusion problem (color figure available online).

5.1. Smith and Hutton Problem

The problem of Smith and Hutton [23] will be investigated in a divergence-free flow field with $u = 2y(1 - x^2)$ and $v = -2x(1 - y^2)$ shown in Eq. (1). In Figure 4, the boundary condition along the inlet $-1 \le x \le 0$, $y = 0$, is prescribed by $\phi = 1 + \tan h[10(2x + 1)]$. Along the lines $x = -1$, $y = 1$, and $x = 1$, ϕ is prescribed as $1 - \tan h(10)$, while along the outlet ($0 \le x \le 1$, $y = 0$), a zero gradient condition is specified.

For the case investigated at $\mu = 10^{-4}$, the results will be calculated at $\Delta x = \Delta y = 1/40$. As Figure 5*a* shows, the oscillatory solution predicted from the center-type scheme using the kernel function given in (19) is under our expectation, since this center-type scheme suffers from numerical instability when solving the convection-dominated problem [24]. In order to suppress the instability problem,

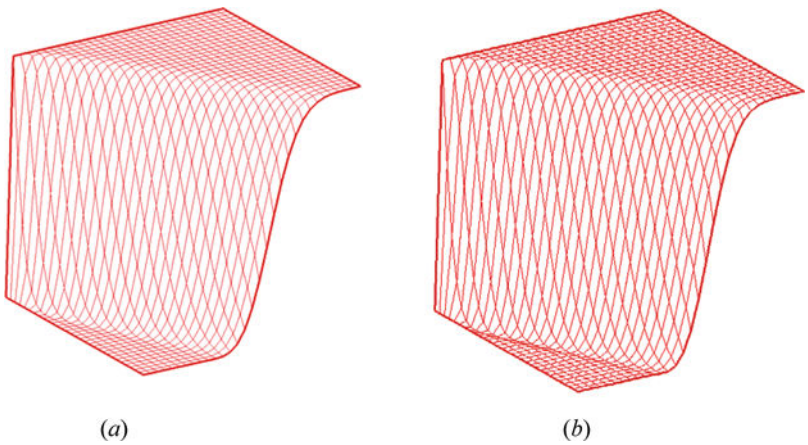

Figure 8. Predicted nonoscillatory solution profiles for the skew advection-diffusion problem investigated at two different values of μ: (*a*) $\mu = 10^{-3}$; (*b*) $\mu = 10^{-5}$ (color figure available online).

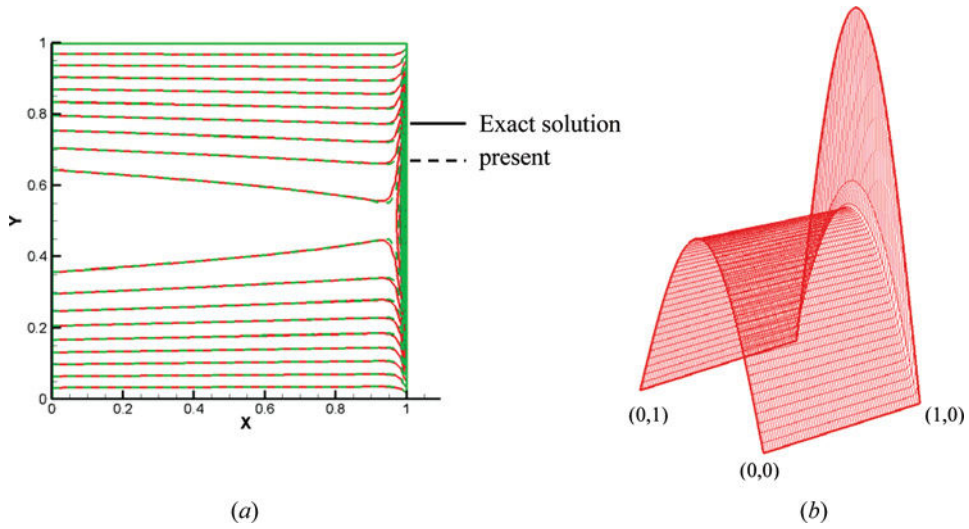

Figure 9. Comparison of exact and predicted solutions for test problem in Section 5.3: (*a*) contour plot of ϕ; (*b*) predicted sharp layer near $x = 1$ and the two boundary layers at $y = 0$ and $y = 1$ (color figure available online).

one can damp out these oscillations by the damping term introduced into the upwind-type particle method (see Figure 5*b*). It can be seen from Figure 6 that the predicted upwind-type solution is essentially nonoscillatory. The efficacy of applying the proposed particle model to simulate high-Peclet-number flow with an interior sharp layer is therefore demonstrated.

5.2. Skew Convection-Diffusion Problem

In Figure 7 the square cavity is divided into two subdomains by the straight line, which passes through (0, 0), with a slope of $\tan^{-1}(v/u)$, where u and v are shown in Eq. (1). We consider in this study the unit velocity vector (u, v), which is parallel to the dividing line, in the 21×21 (for $\mu = 10^{-3}$ and $\mu = 10^{-5}$) uniformly discretized mesh system. Subject to the boundary conditions for the working variable ϕ, one can clearly see from Figure 8 that a shear layer exists in the vicinity of the dividing

Table 4. L_2-error norms and corresponding rates of convergence computed on five meshes using the center-type and upwind-type particle interaction models for the test problem in Section 5.3

Mesh	L_2-error norm, center-type	L_2-error norm, upwind-type	Rate of convergence, upwind-type
60×60	1.034×10^{-2}	7.985×10^{-3}	
70×70	7.437×10^{-3}	5.901×10^{-3}	1.96200
80×80	5.591×10^{-3}	4.534×10^{-3}	1.97345
90×90	4.351×10^{-3}	3.592×10^{-3}	1.97733
100×100	3.480×10^{-3}	2.918×10^{-3}	1.97238

Table 5. Comparison of predicted maximum error and corresponding rate of convergence shown in [$O(h^{\text{rate of convergence}})$] on eight meshes based on upwind particle interaction model for the Gartland test problem

Mesh	DWMA [25]	CDS [26]	SCHOS [26]	Center-type	Upwind-type	Upwind-type L_2-error norm
8×8	3.685×10^{-2}	9.060×10^{-1}	4.248×10^{-1}	9.143×10^{-1}	2.404×10^{-1}	7.799×10^{-2}
16×16	5.812×10^{-2} $O(h^{-0.65737})$	5.618×10^{-1} $O(h^{0.689454})$	1.670×10^{-1} $O(h^{1.34694})$	5.633×10^{-1} $O(h^{0.698764})$	2.890×10^{-1} $O(h^{-0.265633})$	5.601×10^{-2} $O(h^{0.477605})$
32×32	4.993×10^{-2} $O(h^{0.219128})$	2.873×10^{-1} $O(h^{0.967499})$	3.365×10^{-2} $O(h^{2.31117})$	2.876×10^{-1} $O(h^{0.969840})$	1.916×10^{-1} $O(h^{0.592972})$	2.488×10^{-2} $O(h^{1.17070})$
64×64	2.106×10^{-2} $O(h^{1.2454})$	9.493×10^{-2} $O(h^{1.59762})$	3.151×10^{-3} $O(h^{3.41672})$	9.490×10^{-2} $O(h^{1.59958})$	7.301×10^{-2} $O(h^{1.39193})$	7.038×10^{-3} $O(h^{1.82175})$
70×70	N.A.	N.A.	N.A.	7.980×10^{-2} $O(h^{1.93389})$	6.235×10^{-2} $O(h^{1.76129})$	5.901×10^{-3} $O(h^{1.96628})$
80×80	N.A.	N.A.	N.A.	6.095×10^{-2} $O(h^{2.01802})$	4.870×10^{-2} $O(h^{1.85039})$	4.534×10^{-3} $O(h^{1.97345})$
90×90	N.A.	N.A.	N.A.	4.755×10^{-2} $O(h^{2.10788})$	3.873×10^{-2} $O(h^{1.94480})$	3.592×10^{-3} $O(h^{1.97733})$
100×100	N.A.	N.A.	N.A.	3.779×10^{-2} $O(h^{2.18049})$	3.128×10^{-2} $O(h^{2.02766})$	2.918×10^{-3} $O(h^{1.97238})$

line. No oscillatory solution is found to occur in regions near as well as apart from the dividing line.

5.3. Gartland Problem

Finally, we will consider the problem involving a sharply varying solution profile near the boundary along the downstream edge at $x = 1$and two shear layers along the top and bottom edges at $y = 0$ and $y = 1$. This problem with the boundary/shear layers will be investigated in a square of unit length at $(u, v)=(1, 0)$ and $\mu = 10^{-2}$.

The boundary condition is prescribed according to the following exact solution for Eq. (1) [25]:

$$\phi = e^{x/2\mu} \sin \pi y \frac{2e^{-1/2\mu} \sinh \lambda x + \sinh \lambda(1-x)}{\sinh \lambda} \tag{34}$$

Our calculation will be carried out at $u = 1$ and $\lambda = \pi^2 + (1/4\mu^2)$. As Figure 9 shows, near the boundaries $x = 1$, $y = 0$, and $y = 1$, one can clearly see the predicted nonoscillatory high-gradient solution profile. For completeness, we also solve this problem in different meshes so that we can calculate the corresponding rates of convergence, which are approximately equal to the theoretical rate, tabulated in Table 4.

For the sake of making a comparison with other numerical solutions, we also carry out calculations for the case investigated at $\mu = 10^{-2}$ in eight meshes, 8^2, 16^2, 32^2, 64^2, 70^2, 80^2, 90^2, and 100^2. The predicted maximum errors, tabulated in Table 5, are seen to be smaller than those predicted by the second-order-accurate central scheme CDS but larger than those by the DWMA scheme of Gartland [25] and the SCHOS scheme of Gupta et al. [26]. The rates of convergence for the predicted results in Table 5 are seen to be equal to the theoretical rate as well.

6. CONCLUDING REMARKS

As a first step toward accurately simulating the interfacial flow problem by the moving particle method, we developed in this study a kernel function within the nine-point stencil stationary particle framework so as to facilitate theoretical derivation. The idea of developing the proposed particle interaction model is to formulate the kernel function, which accommodates the properties embedded in the smoothed delta function, for the pure diffusion (or Laplace) equation. This center-type kernel function $w(r)$, which is constrained by $\int_{r/r_e=-1}^{r/r_e=1} w(r)\, dr = 1$ in the user's chosen particle interaction circle with radius r_e, will then be modified by adding a flow-direction dependent term to the center-type kernel function. This helps to enhance numerical stability by means of the introduced streamline diffusion term in cases when the convection term becomes increasingly larger than the diffusion term. The way of stabilizing the particle interaction model is to implicitly add a proper amount of diffusion, mainly along the flow direction, so that the upstream particles can be more weighted. To justify the center and upwind kernel functions developed for simulating low- and high-Peclet-number flows, we investigated several well-known benchmark problems. The predicted results clearly show that the

solution predicted by the second-order-accurate upwind-type particle interaction model can capture the interior as well as the boundary layers quite well without showing numerical oscillations in the region with sharp gradients.

REFERENCES

1. C. W. Hirt, A. A. Amsden, and J. L. Cook, An Arbitrary Lagrangian-Eulerian Computing Method for All Flow Speeds, *J. Comput. Phys.*, vol. 14, pp. 227–253, 1974.
2. F. H. Harlow and J. E. Welch, Numerical Calculation of Time-Dependent Viscous Incompressible Flow of Fluid with a Free Surface, *Phys. Fluids*, vol. 8, pp. 2182–2189, 1965.
3. C. W. Hirt and B. D. Nichols, Volume of Fluid (VOF) Method for Dynamics of Free Boundaries, *J. Comput. Phys.*, vol. 39, pp. 201–221, 1981.
4. S. Osher and R. P. Fedkiw, Level Set Methods: An Overview and Some Recent Results, *J. Comput. Phys.*, vol. 169, pp. 463–502, 2001.
5. F. H. Harlow, A Machine Calculation Method for Hydrodynamic Problems, Los Alamos Scientific Laboratory Report LAMS-1956, 1955.
6. L. B. Lucy, A Numerical Approach to the Testing of the Fission Hypothesis, *Astr. J.*, vol. 82, pp. 1013–1024, 1977.
7. R. A. Gingold and J. J. Monaghan, Smoothed Particle Hydrodynamics: Theory and Application To Non-spherical Stars, *Mon. Not. R. Astron. Soc. J.*, vol. 181, pp. 375–389, 1977.
8. J. J. Monaghan, Simulating Free Surface Flows with SPH, *J. Comput. Phys.*, vol. 110, pp. 399–406, 1994.
9. S. Koshizuka, H. Tamako, and Y. Oka, A Particle Method for Incompressible Viscous Flow with Fluid Fragmentation, *CFD Journal*, vol. 4, pp. 29–46, 1995.
10. H. Y. Yoon, S. Koshizuka, and Y. Oka, A Particle-Gridless Hybrid Method for Incompressible Flows, *Int. J. Numer. Meth. Fluids*, vol. 30, pp. 407–424, 1999.
11. J. Liu, S. Koshizuka, and Y. Oka, A Hybrid Particle-Mesh Method for Viscous, Incompressible Multiphase Flows, *J. Comput. Phys.*, vol. 202, pp. 65–93, 2005.
12. B. Ataie-Ashtiani and L. Farhadi, A Stable Moving-Particle Semi-implicit Method for Free Surface Flows, *Fluid Dynam. Res.*, vol. 38, pp. 241–256, 2006.
13. S. Hibi and K. Yabushita, A Study on Reduction of Unusual Pressure Fluctuation of MPS Method, *J. Kansai Soc. N. A. Japan*, vol. 241, pp. 125–131, 2004.
14. M. Sueyoshi, Validation of Numerical Code by a Particle Method for Violent Free-Surface Problems, *Int. J. Offshore Polar Eng.*, vol. 16, pp. 261–267, 2006.
15. A. Khayyer and H. Gotoh, Development of CMPS Method for Accurate Water Surface Tracking in Breaking Waves, *Coast Eng. J.*, vol. 50, pp. 179–207, 2008.
16. A. Khayyer and H. Gotoh, Modified Moving Particle Semi-implicit Methods for the Prediction of 2D Wave Impact Pressure, *Coast. Eng.*, vol. 56, pp. 419–440, 2009.
17. M. Kondo and S. Koshizuka, Improvement of Stability in Moving Particle Semi-implicit Method, *Int. J. Numer. Meth. Fluids*, vol. 65, pp. 638–654, 2011.
18. S. Zhang, K. Morita, K. Fukuda, and N. Shirakawa, An Improved MPS Method for Numerical Simulations of Convective Heat Transfer Problems, *Int. J. Numer. Meth. Fluids*, vol. 51, pp. 31–47, 2006.
19. T. Belytschko, Y. Krongaux, D. Organ, M. Fleming, and P. Krys, Meshless Methods: An Overview and Recent Developments, *Comput. Meth. Appl. Mech. Eng.*, vol. 139, pp. 3–47, 1996.
20. S. Koshizuka and Y. Oka, Moving-Particle Semi-implicit Method for Fragmentation of Incompressible Fluids, *Nucl. Sci. Eng.*, vol. 123, pp. 421–434, 1996.

21. S. Koshizuka, A. Nobe, and Y. Oka, Numerical Analysis of Breaking Waves Using the Moving Particle Semi-implicit Method, *Int. J. Numer. Meth. Fluids*, vol. 26, pp. 751–769, 1998.
22. A. Shakibaeinia and Y. C. Jin, A Weakly Compressible MPS Method for Modeling of Open-Boundary Free-Surface Flow, *Int. J. Numer. Meth. Fluids*, vol. 63, pp. 1208–1232, 2010.
23. R. M. Smith and A. G. Hutton, The Numerical Treatment of Convection—A Performance Comparison of Current Methods, *Int. J. Numer. Meth. Heat Transfer*, vol. 5, pp. 439–461, 1982.
24. J. Zhang and J. J. Zhao, Truncation Error and Oscillation Property of the Combined Compact Difference Scheme, *Appl. Math. Comput.*, vol. 161, pp. 241–251, 2005.
25. E. C. Gartland, Discrete Weighted Mean Approximation of a Model Convection-Diffusion Equation, *SIAM J. Sci. Stat. Comput.*, vol. 3, pp. 460–472, 1982.
26. M. M. Gupta, R. P. Manohar, and J. W. Stephenson, High-Order Difference Schemes For Two-Dimensional Elliptic Equations, *Numer. Meth. Partial Differ. Eqs.*, vol. 1, pp. 71–80, 1985.